Disentangling picosecond events that complicate the quantitative use of the calcium sensor YC3.60

Laptenok, S.; van Stokkum, I.H.M.; Borst, J.W.; van Oort, B.F.; Visser, A.J.W.G.; van Amerongen, H.

published in
Journal of Physical Chemistry B
2012

DOI (link to publisher)
10.1021/jp211830e

document version
Publisher's PDF, also known as Version of record

THE JOURNAL OF PHYSICAL CHEMISTRY B

Article

pubs.acs.org/JPCB

Disentangling Picosecond Events That Complicate the Quantitative Use of the Calcium Sensor YC3.60

S. P. Laptenok,[†,∥,⊥] I. H. M. van Stokkum,[∥] J. W. Borst,[‡,§] B. van Oort,[∥] A. J. W. G. Visser,[‡,§] and H. van Amerongen*[,†,§]

Laboratories of [†]Biophysics and [‡]Biochemistry and [§]Microspectroscopy Centre, Wageningen University, P.O. Box 8128, 6700 ET Wageningen, The Netherlands

[∥]Department of Physics and Astronomy, Faculty of Sciences, Vrije Universiteit Amsterdam, De Boelelaan 1081, 1081 HV Amsterdam, The Netherlands

ABSTRACT: Yellow Cameleon 3.60 (YC3.60) is a calcium sensor based on Förster resonance energy transfer (FRET). This sensor is composed of a calmodulin domain and a M13 peptide, which are located in between enhanced cyan-fluorescent protein (ECFP) and the Venus variant of enhanced yellow-fluorescent protein (EYFP). Depending on the calcium concentration, the efficiency of FRET from donor ECFP to acceptor EYFP is changing. In this study, we have recorded time-resolved fluorescence spectra of ECFP, EYFP, and YC3.60 in aqueous solution with picosecond time resolution, using different excitation wavelengths. Detailed insight in the FRET kinetics was obtained by using global and target analyses of time- and wavelength-resolved fluorescence of purified YC3.60 in calcium-free and calcium-bound conformations. The results clearly demonstrate that for both conformations, there are two distinct donor populations: a major one giving rise to FRET and a minor one not able to perform FRET. The transfer time for the calcium-bound conformation is 21 ps, whereas it is in the order of 1 ns for the calcium-free conformation. Ratio imaging of acceptor and donor fluorescence intensities of YC3.60 is usually applied to measure Ca^{2+} concentrations in living cells. From the obtained results, it is clear that the intensity ratio is strongly influenced by the presence of donor molecules that do not take part in FRET, thereby significantly affecting the quantitative interpretation of the results.

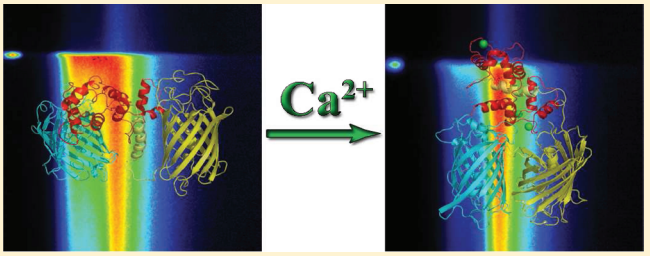

INTRODUCTION

Genetically encoded sensors have become powerful tools for investigating cellular signaling pathways. Cellular processes can even be visualized in real time through the use of sensors that are based on the green-fluorescent protein (GFP)[1] or its variants for specific intracellular constituents.[2,3] Many of these sensors use changes in Förster resonance energy transfer (FRET) efficiency between donor and acceptor variants of GFP separated by a ligand binding domain that is sensitive to the presence of a particular (signaling) molecule.

FRET is a photophysical process in which the excited-state energy is transferred nonradiatively from a donor molecule to an acceptor molecule at close distance (<10 nm) via weak dipole−dipole coupling.[4] The energy transfer rate is inversely proportional to the sixth power of the distance (R) between donor and acceptor. Since FRET only occurs between molecules in close proximity, it can be used as a spectroscopic method to investigate interactions of and conformational changes in biological macromolecules.[5,6] Since recently, improved opto-electronic technology in cell biology[7,8] allows imaging of biological processes in living cells with high speed and accuracy using genetically encoded fluorescence sensors.

Changes in free calcium concentration play an important role in many biological processes since calcium is an important second messenger in intracellular signal transduction. Therefore, much effort has been spent on the development of systems for imaging calcium fluxes. The creation of genetically encoded fluorescent protein sensors for measuring intracellular Ca^{2+} has the potential to enable studies of calcium signaling in vivo, which are difficult or impossible with the widely used chemically synthesized fluorescent indicators.[9,10] Cameleon sensors are fluorescent calcium indicators composed of genetically encoded protein constructs without any cofactors.[10,11] The cameleon variant YC3.60 is a fusion of an enhanced cyan-fluorescent protein (ECFP, donor) and an enhanced yellow-fluorescent protein (EYFP) derivative (Venus) moiety (acceptor) linked by calmodulin and a calmodulin binding peptide of myosin light chain kinase (M13). YC3.60 has been genetically optimized to have the largest dynamic range of ratio imaging of EYFP/ECFP emissions resulting in the most sensitive calcium sensor.[12] The binding of calcium ions to calmodulin makes calmodulin wrap around the M13 domain increasing the efficiency of FRET from ECFP to Venus. However, for a correct

Received: December 8, 2011
Revised: February 5, 2012
Published: February 9, 2012

quantitative analysis of the data observed for live cells, an accurate study of the fluorescence dynamics of sensors in vitro, which up to now has been missing, is required.

A number of methods have been developed to detect FRET,[5] but quantitative analysis is rather complicated in most cases, and various errors can occur. As was recently reported, the detection of the fluorescence rise time for the acceptor molecules upon donor excitation provides the most accurate estimation of the transfer rates/efficiencies.[13,14] In these studies, FRET was studied using simultaneous analysis of time-resolved fluorescence of donor and acceptor at two, discrete wavelengths. Although the method provides more accurate estimates of the transfer rate(s), spectral information is strongly limited and therefore not all processes can be addressed, for instance, the photoconversion of the acceptor into donor-like species.[15,16] In the present study, we have studied YC3.60 with and without calcium with a picosecond synchroscan fluorescence detection system (streak camera), which allowed the recording of fluorescence spectra with picosecond time resolution, and subsequent detailed data analysis.

MATERIALS AND METHODS

Protein Material, Sample Preparation. cDNA of YC3.60 was kindly provided by Dr. Atsushi Miyawaki (RIKEN Brain Science Institute, Saitama, Japan). The full length sensor was cloned into the GST fusion vector (pGEX5 ×2 vector). The YC3.60 was isolated and purified as previously described.[13,17] The purity of the YC3.60 protein was analyzed on SDS-PAGE, and a single band of approximately 75 kDa without degradation products was observed.

Time-Resolved Fluorescence Using the Streak-Camera Setup. Picosecond fluorescence spectra measurements were performed using a synchroscan streak-camera system. Excitation light pulses were obtained with a set of lasers and optical amplifiers from Coherent Inc., Santa Clara, CA, USA. A mode-locked Ti:Sapphire laser model Mira 900 was used to generate short light pulses of 800 nm with an average power of 0.5 W, duration of about 200 fs, and repetition rate of 79.5 MHz. A small fraction of the output of this laser was used for synchronization of the sweep field in the streak camera, while the major part was fed into a regenerative amplifier model RegA 9000, where the energy of the pulses is increased, while the repetition rate is decreased to 250 kHz. Continuous wave solid state lasers (Coherent Verdi V5 and Coherent Verdi V10) were used to pump the Mira and RegA, respectively. The output of the RegA was directed to an optical parametric amplifier (OPA 9400), which was used to produce excitation pulses, at 350 and 400 nm. The light intensity was attenuated with neutral density filters, and residual white light of the OPA was removed with an interference filter. Vertical polarization of the excitation light was set with a Berek polarizer model 5540 (New Focus, San Jose, CA, USA). A lens with a focal length of 15 cm focused the light into a 150 μm spot in a static quartz cuvette of 1.0 × 0.4 cm at room temperature. In front of the streak camera, an imaging spectrograph was mounted (model 250is, Chromex, Albuquerque, NM, USA). Fluorescence emission was focused into the input slit of the spectrograph, using two identical achromatic lens assemblies (model UV APO special; f = 70 mm; d = 22 mm; Sill Optics, Wendelstein, Germany) placed in a complementary manner with a Glan Taylor polarizer (model GT20, Leysop Ltd., Essex, England) and an optical long-pass filter (408 nm) in between, to suppress light scatter. The detection polarizer was set at a magic angle orientation relative to the polarization of the excitation. The output of the spectrograph was coupled directly onto the stripe-shaped (height 70 μm) cathode of the streak-camera (model C5680 with model M5675 Synchroscan unit, Hamamatsu Photonics K.K., Hamamatsu City, Japan). The wavelength dispersion of the spectrograph was in the horizontal direction; the time dispersion of the streak tube was in the vertical direction. For more technical details see refs 18−21.

Collection of Streak Images. Streak images of YC3.60 in a Ca^{2+}-free and Ca^{2+}-bound conformations were measured upon excitation with 400 nm and 350 nm laser, with 60 μW or 100 μW average power, respectively. Streak images obtained with the CCD camera were corrected for nonlinearity of the time- and wavelength axes and the sensitivity of the detection system. Images were measured with a 2 ns time window, and the spectral window ranged from 450 to 650 nm. The acquisition time of one image was about 20 min. To increase the signal-to-noise ratio, decays were averaged over 4 nm before analysis. All measurements were performed with 1 μM concentration of protein in either 5 mM PBS (pH = 7.4) or 100 mM Hepes (pH = 7.9) at 20 °C.

Data Analysis. The measured images (fluorescence intensity as a function of time and wavelength) were corrected for the presence of time jitter, background, and shading using the high performance digital temporal analyzer (HPDTA, Hamamatsu Photonics). In these images, fluorescence detected directly after excitation shows overlap with fluorescence after 6.3 ns (due to the streak-camera backsweep; for more details see refs 21 and 22). This property was used during data analysis to obtain information about slow relaxation processes. In addition to fluorescence, the images upon 400 nm excitation show the presence of Raman scatter (around 465 nm), overlapping with the fluorescence spectra. Scatter was included in the fitting model as a component with an infinitely fast decay.

The aim of the analysis is to obtain a model-based description of the time-resolved data in terms of a small number of precisely estimated rate constants and fluorescence spectra. This was achieved by global analyis. The basis for global analysis is the superposition principle, which uses the assumption that the measured data result from a linear combination of n_{comp} components, each with a distinct time profile and spectrum. Global analysis was applied in two ways: first, the data were fitted to a parallel model in which n_{comp} excited species decay monoexponentially in parallel with n_{comp} rate constants k_i. In this procedure, spectral shapes are left unconstrained yielding decay associated spectra (DAS). Second, the data were fitted to a full compartmental scheme (the target model), which includes all possible branching routes and equilibria between compartments. This allows estimating the spectra of each of the excited species (species associated spectra, SAS). For more details about the use of compartmental models for global and target analysis of time-resolved spectroscopy data see reviews by van Stokkum and co-workers.[21,22] For details on parameter estimation techniques see refs 23−25. Analysis was performed using open-source software called Glotaran, a problem solving environment for fitting superposition models to multidimensional data (http://glotaran.org).[26]

RESULTS AND DISCUSSION

Experiment with ECFP Only. ECFP is known to show biexponential fluorescence decay behavior due to two different conformations of the chromophore in the protein, a minor population with quenched fluorescence and a major population with nonquenched fluorescence.[27−30] A biexponential fluorescence decay analysis of ECFP showed that the shorter lifetime (1.0 ns) contributed for 33% and the longer lifetime (3.6 ns) for 67%.[28] To quantify the biexponential decay, control experiments with ECFP only were performed using 350 and 400 nm excitation. The DAS estimated from global analysis of the streak images of ECFP are presented in Figure 1.

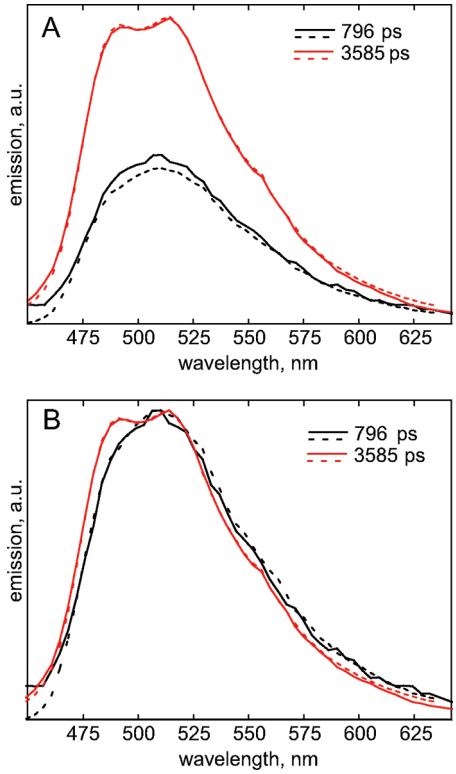

Figure 1. DAS (A) and DAS normalized to the emission maxima (B) of ECFP alone obtained after global analysis of streak-camera data (ECFP fluorescence measured upon 400 nm and 350 nm excitation). The corresponding lifetimes are given in the figure. Dashed lines represent excitation at 400 nm; solid lines, excitation at 350 nm.

The presence of Ca^{2+} does not affect the fluorescence decay of ECFP (data not shown). Irrespective of the excitation wavelength, analysis of the ECFP streak images shows the presence of 2 components with the lifetimes of 796 and 3585 ps. Also, the shape of the component spectra does not depend on excitation wavelength. The spectral shapes of both components are somewhat different from each other. However, in the YC3.60 construct, both ECFP populations are potential donors of excitation energy to EYFP leading to reduction of both lifetimes, given the good overlap between both fluorescence spectra with the absorption spectrum of EYFP. The rate constant of energy transfer should be the same for both types of ECFP molecules, but the transfer efficiency of ECFP with shorter fluorescence lifetime is smaller than that of nonquenched ECFP.

Experiment with EYFP Only. The presence of Ca^{2+} does not show any effect on the EYFP fluorescence (data not shown). However, it has been reported from acceptor photobleaching experiments that EYFP can be photoconverted into a species with fluorescence in the same region as ECFP.[15,16] Therefore, experiments with EYFP only were performed to resolve the lifetime(s) and spectrum of this species. Figure 2 shows the DAS resulting from global analysis of the EYFP fluorescence upon excitation at either 350 or 400 nm.

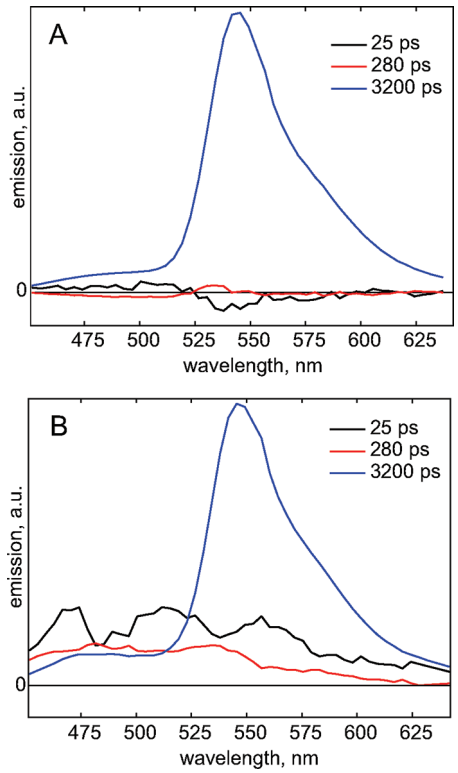

Figure 2. DAS of EYFP obtained after global analysis of streak-camera data. The corresponding lifetimes are given in the figure. The excitation wavelength was 350 nm (A) and 400 nm (B). The average excitation power was about 250 μW.

It is clear that a species with a broad spectrum and complicated decay kinetics is present upon 400 nm excitation, while upon 350 nm excitation, its contribution is negligible. We ascribe this component to a photoconverted form of EYFP. Both excitation wavelengths are at the very blue edge of the absorption spectrum of EYFP. However, at 400 nm, the absorption cross-section of EYFP is larger than at 350 nm, and more photoconversion can be expected. The relative contribution of the fast components is increasing upon increasing the excitation light energy (data not shown). The lifetimes of 25 ps (black) and 280 ps (red) are close to the fast lifetimes observed for YC3.60 molecules in the Ca^{2+}-bound conformation (see below). These experiments clearly show that photoconverted EYFP in YC3.60 would remove its acceptor properties and allow to exhibit ECFP unquenched fluorescence lifetimes.

Experiments with YC3.60. There is a substantial change in the relative distance between the ECFP and EYFP chromophores in YC3.60 upon binding of Ca^{2+} to calmodulin, which is reflected in a shortening of the lifetime of the ECFP chromophores and a faster rise of the fluorescence of the EYFP chromophore due to faster excitation energy transfer.[13] The

dx.doi.org/10.1021/jp211830e | J. Phys. Chem. B 2012, 116, 3013−3020

present study extends the work of Borst and co-workers[13] by adding the spectral dimension. Moreover, the experiment was now also performed at 350 nm excitation, which shifts the Raman scatter peak to 400 nm, avoiding overlap with the fluorescence spectrum of ECFP. A disadvantage is that the absorption cross-section of ECFP is rather low at 350 nm, and moreover, a significant amount of EYFP is excited directly at this wavelength. This is, however, taken into account in the data analysis, and the rapid transfer processes occurring in the system are not affected by Raman scatter and therefore can be resolved more accurately.

Representative traces of YC3.60 in the Ca^{2+}-free and Ca^{2+}-bound conformation detected at 480 and 560 nm are depicted in Figure 3. At 480 nm, the emission is mostly due to fluorescence from ECFP molecules. The fluorescence detected at 560 nm mainly stems from EYFP molecules. The fluorescence kinetics at that wavelength (blue and green traces) does not depend on the excitation wavelength, both in the Ca^{2+}-bound and Ca^{2+}-free conformation.

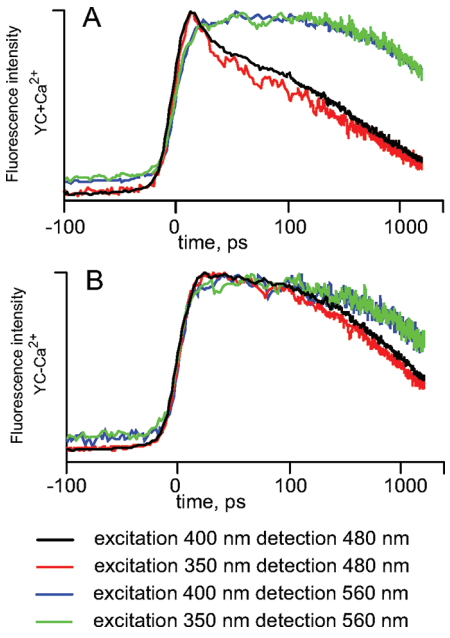

Figure 3. Peak-normalized decay traces of the fluorescence of YC3.60 at 480 and 560 nm, after excitation at 400 nm (black and blue) and 350 nm (red and green). The fluorescence is averaged over 4 nm. Panel A represents traces of the Ca^{2+}-bound conformation of YC3.60. Panel B represents the traces of YC3.60 in the Ca^{2+}-free conformation. Note that the time axis in both panels is linear from −100 to 100 ps and logarithmic thereafter.

Figure 3 reflects the situation described in ref 13, where two detection wavelengths (480 and 560 nm) and one excitation wavelength (400 nm) were used. The fluorescence at 480 nm (red and black traces) decays much faster for the Ca^{2+}-bound conformation of YC3.60 than for the Ca^{2+}-free conformation of YC3.60, which is due to faster excitation energy transfer in the former case. For the Ca^{2+}-free conformation of YC3.60, the fluorescence detected at 480 nm disappears somewhat faster upon 350 nm excitation (red trace) than upon 400 nm excitation (black trace). This difference is slightly more pronounced for the Ca^{2+}-bound conformation, although the very first parts of the traces are very similar for both excitation wavelengths, indicating that the fast energy transfer is identical for both excitation wavelengths. The deviation at later times must correspond to a different unidentified process.

Decay Associated Spectra. Streak images of the Ca^{2+}-bound conformation of YC3.60 upon 350 and 400 nm excitation were analyzed globally (i.e., the lifetimes were assumed to be equal for both experiments). The analysis leads to three components with lifetimes of 20, 430, and 2870 ps. Analysis of the images of YC3.60 in the Ca^{2+}-free conformation leads to three components with lifetimes of 80, 795, and 3000 ps. Figure 4 shows the estimated DAS for the Ca^{2+}-free and Ca^{2+}-bound conformations of the YC3.60 upon excitation at 350 and 400 nm. Spectra in panels A and B are normalized to the maximum of the EYFP fluorescence in order to emphasize relative contributions of the components, while in panels C and D, spectra are normalized to their maximum values in order to emphasize spectral shapes. Solid lines represent analysis of experimental data upon 400 nm excitation, and dashed lines represent analysis of experimental data upon 350 nm excitation.

Energy transfer in the Ca^{2+}-bound conformation (Figure 4A,C) is characterized by the black 20 ps and red 430 ps DAS. Both DAS have positive amplitudes (below ~520 nm), corresponding to fluorescence decay, and negative amplitudes (above ~520 nm), corresponding to fluorescence rise, which should be interpreted as energy transfer from ECFP to EYFP. However, the spectra are not conservative: the area of the positive part of the spectrum is bigger than that of the negative part, and apparently, an (unknown) decay process occurring with a similar rate as the energy transfer process takes place. In both experiments, the fast component with a lifetime of 20 ps dominates the transfer kinetics, and it can be attributed to energy transfer in the Ca^{2+}-bound conformation of the YC3.60. The second transfer component with the smaller amplitude (lifetime of 430 ps) is attributed to a small fraction of the YC3.60 population in the Ca^{2+}-free conformation. Given the used concentration of YC3.60 of 1 μM and the earlier reported apparent dissociation constant for Ca^{2+}-binding of 250 nM,[12] such small fraction is likely to be present. The long-lived DAS (blue) with a lifetime of 2870 ps can be attributed to a mixture of EYFP and noninteracting ECFP chromophores (mainly below ~520 nm). In the Ca^{2+}-bound conformation, there are two major rise components present in the EYFP fluorescence region with different time constants, while in the Ca^{2+}-free conformation, there is only one slow rise component (red DAS) with a long lifetime of 795 ps (Figure 4B,C). The negative part of the spectrum is small, which can be explained by the fact that the fast decaying component of ECFP alone (Figure 1) is almost identical to the transferring component, and therefore, the amplitude of these rise and decay processes almost cancel. However, a fast decay component with a 80 ps lifetime and a broad spectrum (black) are present that do not correspond to energy transfer or represent energy transfer and another process with similar lifetimes, and therefore, the amplitudes of these processes are compensating each other. The DAS with a lifetime of 3000 ps (blue) represents a mixture of the fluorescence decay of EYFP and nontransferring ECFP chromophores.

The amplitude ratio of the fluorescence of ECFP and EYFP-Venus depends on the excitation wavelength. In experiments with 350 nm excitation, the relative amplitude of the fluorescence at 560 nm, which is largely due to EYFP, is higher than upon 400 nm excitation. This can be explained by differences in the relative absorption cross-sections at 350 and 400 nm excitation for ECFP and EYFP chromophores (at 350

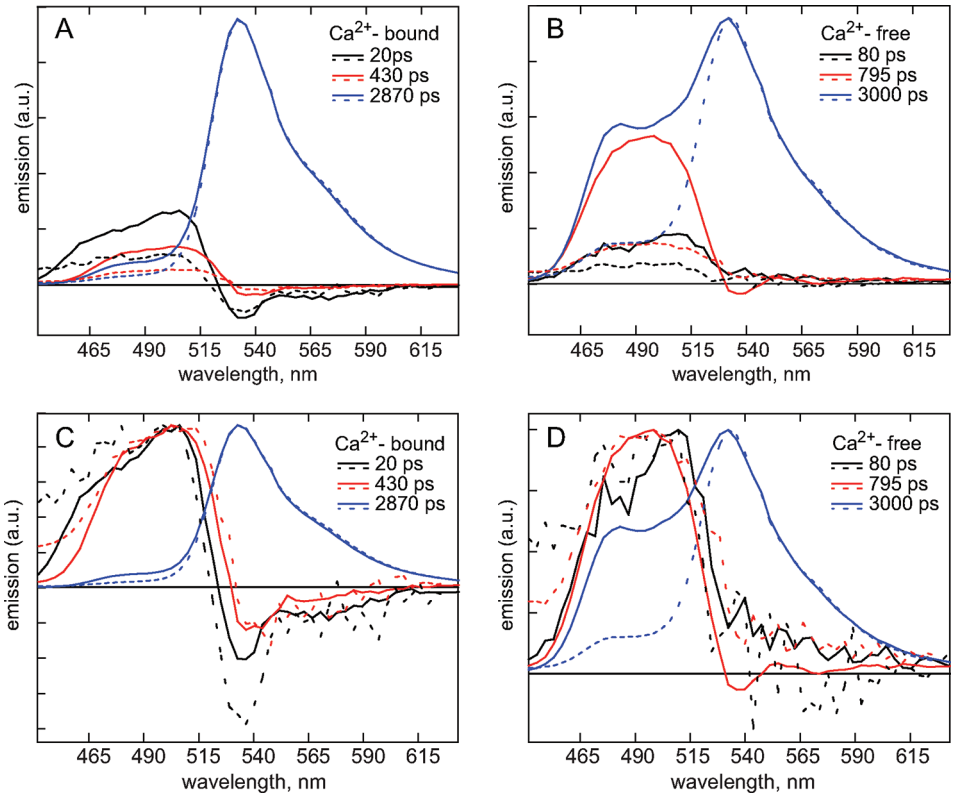

Figure 4. DAS of YC3.60 in Ca^{2+}-bound (A,C) and Ca^{2+}-free (B,D) conformations, obtained after global analysis of streak-camera data. The corresponding lifetimes are given in each panel. The excitation wavelength was 400 nm (solid lines) and 350 nm (dashed lines). Panels A and B represent DAS normalized to the maximum of the EYFP fluorescence. Panels C and D represent DAS normalized to their maximum values. Errors are about 10%.

nm the relative absorbance of both fluorescent proteins are almost the same, while at 400 nm, the absorbance of ECFP is much larger than that of EYFP (data not shown))

A fraction of nontransferring ECFP can be observed independently of the presence or absence of Ca^{2+}. The presence of noninteracting donor molecules can be explained, for example, by the presence of a small population of protonated acceptor chromophores in the construct, which will lead to decreased overlap between donor fluorescence and acceptor absorption spectra.[13] Another explanation can be the presence of photoconverted EYFP molecules. Not only does photobleaching of EYFP result in the loss of the 514 nm absorbance but also new absorption peaks appear in the 390–420 nm region overlapping with the absorption of ECFP.[31] In addition, acceptor photobleaching experiments have shown that the photoproduct of EYFP leads to weak emission in the range 435–480 nm, when excited at 420 nm.[15,16] These photoconverted acceptor molecules are no longer capable to function as FRET acceptors.

Target Analysis. In order to resolve the spectral shape of the various kinetic components observed for YC3.60, target analysis of the data was performed as described before.[22,32] For target analysis, at least five compartments were required to obtain a satisfactory description of the data, and Figure 5 shows the kinetic schemes that were used.

Let us first describe the target analysis of Ca^{2+}-bound YC3.60 (Figure 5A). Compartments 1, 2, 3, and 4 represent interacting and noninteracting ECFP species, and therefore, the spectra of those compartments are assumed to be the same. Compartment 5 corresponds to the EYFP. It can be directly excited at either 400 or 350 nm, whereas the remainder of the excitations results from energy transfer from compartments 1 and 2 with two transfer rates k_{15} and k_{25}, respectively. We have two compartments arising from two populations of ECFP involved in FRET: one major one arising from efficient FRET with transfer time of 20/21 ps and a minor one arising from the presence of Ca^{2+}-free YC3.60 with transfer time of 356/472 ps (Table 1). The presence of Ca^{2+}-free YC3.60 is not surprising because of the used protein concentration and the apparent dissociation constant for the Ca^{2+}- YC3.60 complex (see previous section). Compartments 3 and 4 represent populations of ECFP that do not participate in energy transfer. Two different decay rates are needed representing two different conformations of the chromophores in the protein, a minor population with quenched fluorescence and a major population with nonquenched fluorescence.[27−30] The contribution of quenched ECFP (compartment 3) participating in FRET will be completely hidden in compartment 1 because of the following reason: the Ca^{2+}-bound conformation of YC3.60 has an interchromophoric distance of 2.6 nm[13] yielding an energy transfer efficiency that approaches 100% for both quenched and unquenched ECFP populations. The fluorescence lifetimes of both populations will be dominated by the transfer time of 20 ps.

For Ca^{2+}-free YC3.60, the dominating transfer component has a lifetime of 1097 ps/1451 ps (at 350 nm/400 nm excitation, respectively, Table 1), which is close to the previously reported transfer time of 1.4 ns for YC3.60 in the Ca^{2+}-free conformation.[13] The unquenched ECFP (compartment 4) is mainly responsible for energy transfer because of the

dx.doi.org/10.1021/jp211830e | J. Phys. Chem. B 2012, 116, 3013–3020

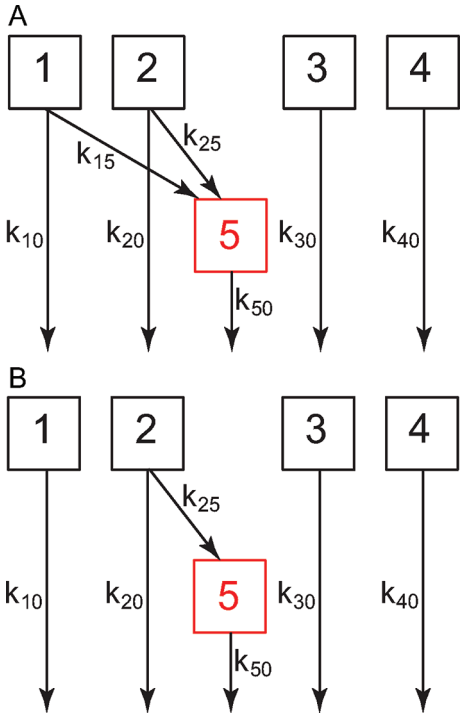

Figure 5. Compartmental scheme that was used for the target analysis of Ca^{2+}-bound YC3.60 (A) and Ca^{2+}-free YC3.60 (B). Compartments 1, 2, 3, and 4 in scheme A are assigned to ECFP fluorescence, while in scheme B, compartment 1 is assigned to the photoproduct of EYFP. Compartment 5 is assigned to EYFP. All compartments can be excited with an excitation pulse with different probability. Rate constants k_{30} and k_{40} represent decay rates to the ground state of the noninteracting ECFP molecules. Rate constant k_{50} represents the decay rate to the ground state of EYFP molecules. Rate constants k_{15} and k_{25} represent transfer rates to EYFP molecules. Rate constants k_{10} and k_{20} in Ca^{2+}-bound YC3.60 and k_{20} in Ca^{2+} -free YC3.60 represent decay rates to the ground state of the interacting ECFP molecules and include contribution from rates k_{30} and k_{40}. The contribution is irresolvable for the present set of data.

following reasons. In the Ca^{2+}-free YC3.60 conformation, the distance between the chromophores is 4.9 nm,[13] which is virtually identical to the Förster radius of 4.9 nm[33] for the ECFP–EYFP FRET pair. However, the latter critical distance was calculated for an average population of ECFP (70% unquenched + 30% quenched). The population of quenched ECFP will have a smaller Förster radius due to its smaller quantum yield and therefore will contribute less to the energy transfer in the Ca^{2+}-free configuration of YC3.60. The transfer efficiency in the latter case would be 20% (Förster radius is 3.9 nm) and will be significantly smaller compared to the efficiency of transfer between the unquenched ECFP and the Venus acceptor (efficiency is 59%; Förster radius is 5.2 nm). After target analysis, there is no sign at all for the characteristic transfer time of 21 ps, which excludes the presence of Ca^{2+}-bound YC3.60. In contrast, a second faster pathway of 89 ps/129 ps (at 350 nm/400 nm excitation, respectively, Table 1) is present and most likely can be attributed to a population of photoconverted EYFP molecules. Two compartments are from both populations of ECFP not participating in FRET (quenched ECFP and unquenched ECFP) and the fifth arising from directly and via FRET excited acceptor molecules. Altogether, there are 5 compartments, but only one is involved in FRET (Figure 5B).

Table 1. Excited-State Lifetime Estimates of YC3.60 in Ca^{2+}-Bound and Ca^{2+}-Free Conformations Obtained from Target Analysis of Streak Images Measured upon 350 and 400 nm Excitation[a]

	excitation 350 nm			excitation 400 nm		
	τ (ps)	directly excited fractions		τ (ps)	directly excited fractions	
		Ca^{2+}-Bound				
comp1: YC3.60 in Ca^{2+}-bound conformation $(k_{10} + k_{15})^{-1}$	20	0.175	***0.583***	21	0.386	***0.551***
comp2: YC3.60 in Ca^{2+}-free conformation $(k_{20} + k_{25})^{-1}$	356	0.061	***0.203***	472	0.186	***0.266***
comp3: quenched ECFP k_{30}^{-1}	690	0.021	***0.07***	781	0.027	***0.039***
comp4: unquenched ECFP k_{40}^{-1}	3472	0.043	***0.143***	3597	0.101	***0.144***
comp5: (EYFP) k_{50}^{-1}	2850	0.7		2791	0.3	
		Ca^{2+}-Free				
comp1: photoproduct k_{10}^{-1}	89	0.058		129	0.092	
comp2: YC3.60 in Ca^{2+}-free conformation $(k_{20} + k_{25})^{-1}$	1097	0.104	***0.43***	1451	0.311	***0.51***
comp3: quenched ECFP k_{30}^{-1}	633	0.046	***0.19***	633	0.099	***0.16***
comp4: unquenched ECFP k_{40}^{-1}	3597	0.092	***0.38***	3597	0.198	***0.33***
comp5: EYFP k_{50}^{-1}	2849	0.7		2909	0.3	

[a]Values in bold–italic are the sum of the fractions of the compartments assigned to ECFP fluorescence normalized to 1.0. Errors are about 10%. Separate estimations of k_{10} and k_{15}, as well as k_{20} and k_{25}, when appearing in pairs, are numerically impossible with the present set of data. Therefore, only lifetimes of the excited states are reported.

Figure 6 shows the species associated spectra (SAS) of YC3.60 estimated from the target analysis (Figure 6A,C for Ca^{2+}-bound YC3.60; Figure 6C,D for Ca^{2+}-free YC3.60).The red trace represents the estimated spectrum of EYFP in YC3.60. The black trace represents estimated spectra of the ECFP populations in YC3.60. Dashed traces represent the steady-state fluorescence spectra of ECFP (black) and of EYFP (red). The spectra of the species estimated from the target analysis are considered to be in relatively good agreement with the steady-state spectra of ECFP and EYFP, although there is a misfit in some cases, especially upon 400 nm excitation, suggesting the presence of some unresolved kinetic processes.

The estimated excited-state lifetimes for the compartments and their starting concentrations, reflecting the amount of direct excitation of the compartments, are summarized in Table 1. It must be noted that separate estimations of rate constants k_{10} and k_{15}, as well as k_{20} and k_{25}, when appearing as pair, are numerically impossible with the present set of data. Therefore, only lifetimes of the excited states are reported in Table 1.

The large differences in the kinetics for Ca^{2+}-free and Ca^{2+}-bound YC3.60 can now be explained. For the Ca^{2+}-bound conformation of YC3.60, very fast transfer is dominating the kinetics (large directly excited fractions of ECFP). Starting concentrations of this ultrafast transfer compartment are very similar for the 350 nm excitation and 400 nm excitation experiments. However, the lifetime of this component is comparable to the half-width of the instrumental response function of the setup (23 ps), and Raman scatter is present in the same wavelength region upon 400 nm excitation.

dx.doi.org/10.1021/jp211830e | J. Phys. Chem. B 2012, 116, 3013–3020

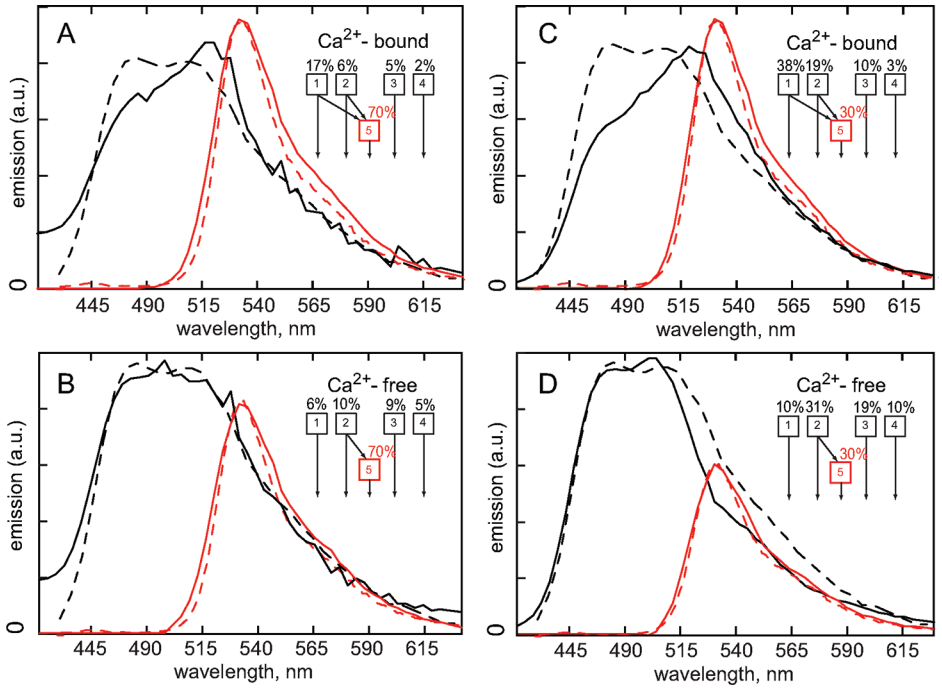

Figure 6. SAS of YC3.60 in Ca^{2+}-bound (A,C) and Ca^{2+}-free (B,D) conformations, obtained after target analysis of streak-camera data. The excitation wavelength was 350 nm (A,B) and 400 nm (C,D). Dashed lines represent steady-state spectra of ECFP (black) and EYFP (red). Percentages mentioned in the scheme represent starting concentrations of the components.

Therefore, the precision of estimating this rate constant is higher in the experiments with 350 nm excitation light.

The amount of noninteracting ECFP in Ca^{2+}-free YC3.60 (compartments 3 and 4) is about twice as large as in the Ca^{2+}-bound case. This result can be explained, in part, by the fact that the population of quenched ECFP participating in FRET will emit with a lifetime in the order of 600 ps, slightly smaller than the lifetime of 700 ps in the absence of FRET. This population cannot be resolved in the target analysis and would increase the relative population of quenched ECFP with respect to that of unquenched ECFP.

CONCLUSIONS

In nearly all cases FRET pairs that consist of visible fluorescent protein are not ideal because there is always a population of nontransferring donor molecules present. Possible reasons have been discussed by Visser and co-workers.[34] It has been reported that most of the fluorescent proteins used as acceptors in microscopic FRET studies can be photoconverted into species that yield fluorescence in the donor spectral region.[15,16,35] Because of their photolability, the generation of photoproducts of fluorescent proteins cannot be avoided under normal experimental conditions. This complicates quantitative analysis of microscopic results. In addition, depending on the protein concentration and apparent dissociation constant of the Ca^{2+} ligand, one should be aware of the presence of two protein populations: one bound with a ligand molecule and another one having no ligand bound. Therefore, time-resolved fluorescence experiments like the ones that were performed in the present study are required for distinguishing between various fractions of transferring and nontransferring donor molecules and photoconverted acceptor molecules enabling quantitative analysis of FRET data. In (steady-state) fluorescence ratio imaging measurements, the presence of a non-FRETing population of donor molecules induced by possibly photoconverted acceptor molecules can lead to underestimation of the FRET efficiency and thus to misinterpretation of the results. This can be nicely illustrated by reported steady-state fluorescence intensity ratio measurements of EYFP (530 nm) and ECFP (480 nm) in YC3.60.[12] In the calcium-bound YC3.60, a maximal ratio R_{max} = 9.3 was found, whereas in the calcium-free YC3.60 a minimal ratio R_{min} = 1.4 was reported.[12] From time-resolved measurements, it is possible to obtain the same information by calculating the ratio of the fluorescence lifetimes of acceptor and donor in the same YC3.60. For calcium-bound YC3.60, the ratio between the average lifetimes of EYFP and ECFP is 4.0 (average lifetime is calculated using estimated lifetimes and relative concentrations from Table 1). However, when the noninteracting fraction is excluded (taking into account two transfer populations), the average fluorescence lifetime of interacting ECFP in that case is 137 ps (see Table 1), leading to R_{max} = 20. When the sole process is ultrafast FRET with a fluorescence lifetime of 20 ps, then one would even observe R_{max} = 140 (see Table 1), which is an order of magnitude larger. Therefore, we must conclude that the observed upper limit of R_{max} must be due to a population of donor molecules in YC3.60 that do not take part in FRET. For calcium-free YC3.60, the difference between the observed ratio (R_{min} = 1.4) and the calculated one (R_{min} = 2, see Table 1) is much smaller. A strategy to improve the calcium sensor YC3.60 for time-resolved fluorescence spectroscopy experiments and to simplify the associated quantitative analysis is to use the CFP variant mTurquoise as the donor molecule, which shows a monoexponential fluorescence decay (3.8 ns) and a fluorescence quantum yield even larger than 0.8.[36]

dx.doi.org/10.1021/jp211830e | J. Phys. Chem. B 2012, 116, 3013–3020

AUTHOR INFORMATION

Corresponding Author

*Phone +31 317 482634. Fax +31 317 482725. E-mail: Herbert.vanAmerongen@wur.nl.

Present Address

[⊥]Laboratoire d'Optique et Biosciences, CNRS UMR 7645, INSERM U696, Ecole Polytechnique, F-91128 Palaiseau, France.

Notes

The authors declare no competing financial interest.

ACKNOWLEDGMENTS

This work was supported by The Netherlands Organization for Scientific Research (NWO) through Computational Science Grant 635.000.014 (to S. P. L.) and a Rubicon Grant (to B.v.O.).

REFERENCES

(1) Tsien, R. Y. *Annu. Rev. Biochem.* **1998**, *67*, 509−544.
(2) Guerrero, G.; Isacoff, E. Y. *Curr. Opin. Neurobiol.* **2001**, *11*, 601−607.
(3) Zhang, J.; Campbell, R. E.; Ting, A. Y.; Tsien, R. Y. *Nat. Rev. Mol. Cell. Biol.* **2002**, *3*, 906−918.
(4) Förster, T. *Z. Naturforsch.* **1949**, *4a*, 321−327.
(5) Jares-Erijman, E. A.; Jovin, T. M. *Curr. Opin. Chem. Biol.* **2006**, *10*, 409−416.
(6) Stryer, L. *Annu. Rev. Biochem.* **1978**, *47*, 819−846.
(7) Agronskaia, A. V.; Tertoolen, L.; Gerritsen, H. C. *J. Biomed. Opt.* **2004**, *9*, 1230−1237.
(8) Gabriel, B.; Teissié, J. *Eur. Biophys. J.* **1998**, *27*, 291−298.
(9) Baird, G. S.; Zacharias, D. A.; Tsien, R. Y. *Proc. Natl. Acad. Sci. U.S.A.* **2000**, *97*, 11984−11989.
(10) Miyawaki, A.; Llopis, J.; Heim, R.; McCaffery, J. M.; Adams, J. A.; Ikura, M.; Tsien, R. Y. *Nature* **1997**, *388*, 882−887.
(11) Miyawaki, A.; Griesbeck, O.; Heim, R.; Tsien, R. Y. *Proc. Natl. Acad. Sci. U.S.A.* **1999**, *96*, 2135−2140.
(12) Nagai, T.; Yamada, S.; Tominaga, T.; Ichikawa, M.; Miyawaki, A. *Proc. Natl. Acad. Sci. U.S.A.* **2004**, *101*, 10554−10559.
(13) Borst, J. W.; Laptenok, S. P.; Westphal, A. H.; Kühnemuth, R.; Hornen, H.; Visser, N. V.; Kalinin, S.; Aker, J.; van Hoek, A.; Seidel, C. A. M.; Visser, A. J. W. G. *Biophys. J.* **2008**, *95*, 5399−5411.
(14) Laptenok, S. P.; Borst, J. W.; Mullen, K. M.; van Stokkum, I. H. M.; Visser, A. J. W. G.; van Amerongen, H. *Phys. Chem. Chem. Phys.* **2010**, *12*, 7593−7602.
(15) Kirber, M. T.; Chen, K.; Keaney, J. F. *Nat. Methods* **2007**, *4*, 767−768.
(16) Valentin, G.; Verheggen, C.; Piolot, T.; Neel, H.; Coppey-Moisan, M.; Bertrand, E. *Nat. Methods* **2005**, *2*, 801.
(17) Smith, D.; Johnson, K. *Gene* **1988**, *67*, 31−40.
(18) van Oort, B.; Amunts, A.; Borst, J. W.; van Hoek, A.; Nelson, N.; van Amerongen, H.; Croce, R. *Biophys. J.* **2008**, *95*, 5851−5861.
(19) van Oort, B.; Eremeeva, E. V.; Koehorst, R. B. M.; Laptenok, S. P.; van Amerongen, H.; van Berkel, W. J. H.; Malikova, N. P.; Markova, S. V.; Vysotski, E. S.; Visser, A. J. W. G.; Lee, J. *Biochemistry* **2009**, *48*, 10486−10491.
(20) van Oort, B.; Murali, S.; Wientjes, E.; Koehorst, R. B. M.; Spruijt, R. B.; van Hoek, A.; Croce, R.; van Amerongen, H. *Chem. Phys.* **2009**, *357*, 113−119.
(21) van Stokkum, I. H. M.; van Oort, B. F.; van Mourik, F.; Gobets, B.; van Amerongen, H. (Sub)-Picosecond Spectral Evolution of Fluorescence Studied with a Synchroscan Streak-Camera System and Target Analysis. In *Biophysical Techniques in Photosynthesis*; Springer: Dordrecht, The Netherlands, 2008; Vol. *II*, pp 223−240.
(22) van Stokkum, I. H. M.; Larsen, D. S.; van Grondelle, R. *Biochim. Biophys. Acta* **2004**, *1657*, 82−104.
(23) Mullen, K. M.; van Stokkum, I. H. M. *J. Stat. Soft.* **2007**, *18*, 1−46.
(24) van Stokkum, I. H. M.; Bal, H. E. *Concurrency and Computation: Practice and Experience* **2006**, *18*, 263−269.
(25) Mullen, K. M.; van Stokkum, I. H. M. *Numer. Algorithms* **2009**, *51*, 319−340.
(26) Snellenburg, J. J.; Laptenok, S. P.; Seger, R.; Mullen, K. M.; van Stokkum, I. H. M. *J. Stat. Soft.* Accepted for publication.
(27) Bae, J. H.; Rubini, M.; Jung, G.; Wiegand, G.; Seifert, M. H. J.; Azim, M. K.; Kim, J.-S.; Zumbusch, A.; Holak, T. A.; Moroder, L.; Huber, R.; Budisa, N. *J. Mol. Biol.* **2003**, *328*, 1071−1081.
(28) Borst, J. W.; Hink, M. A.; van Hoek, A.; Visser, A. J. W. G. *J. Fluoresc.* **2005**, *15*, 153−160.
(29) Demachy, I.; Ridard, J.; Laguitton-Pasquier, H.; Durnerin, E.; Vallverdu, G.; Archirel, P.; Levy, B. *J. Phys. Chem. B* **2005**, *109*, 24121−24133.
(30) Villoing, A.; Ridhoir, M.; Cinquin, B.; Erard, M.; Alvarez, L.; Vallverdu, G.; Pernot, P.; Grailhe, R.; Mérola, F.; Pasquier, H. *Biochemistry* **2008**, *47*, 12483−12492.
(31) McAnaney, T. B.; Zeng, W.; Doe, C. F. E.; Bhanji, N.; Wakelin, S.; Pearson, D. S.; Abbyad, P.; Shi, X. H.; Boxer, S. G.; Bagshaw, C. R. *Biochemistry* **2005**, *44*, 5510−5524.
(32) Mullen, K. M.; Vengris, M.; Stokkum, I. H. *J. Global Optimization* **2007**, *38*, 201−213.
(33) Hink, M. A.; Visser, N. V.; Borst, J. W.; van Hoek, A.; Visser, A. J. W. G. *J. Fluoresc.* **2003**, *13*, 185−188.
(34) Visser, A. J. W. G.; Laptenok, S. P.; Visser, N. V.; van Hoek, A.; Birch, D. J. S.; Brochon, J. C.; Borst, J. W. *Eur. Biophys. J.* **2010**, *39*, 241−253.
(35) Kremers, G.-J.; Hazelwood, K. L.; Murphy, C. S.; Davidson, M. W.; Piston, D. W. *Nat. Methods* **2009**, *6*, 355−358.
(36) Goedhart, J.; van Weeren, L.; Hink, M. A.; Vischer, N. O. E.; Jalink, K.; Gadella, T. W. J. *Nat. Methods* **2010**, *7*, 137−139.